Variable DC Bus Voltage Control Scheme for the More Electric Aircraft Power Generation System

Seang Shen Yeoh, Mohamed Rashed, Serhiy Bozhko
Department of Electrical and Electronic Engineering
University of Nottingham
Nottinghamshire, United Kingdom
Seang.yeoh@nottingham.ac.uk,
Mohamed.Rashed@nottingham.ac.uk,
Serhiy.Bozhko@nottingham.ac.uk

Mike Sanders
Applied Research & Technology
Meggitt Polymers & Composites
Leicestershire, United Kingdom
Mike.sanders@meggitt.com

***Abstract*— This paper aims to introduce a control scheme that offers variable voltage control for more electric aircraft electrical power systems. This control scheme allows increased power intake to the loads by variation of the bus voltage in addition to other key control functions for a generator system. The load considered is the electro-thermal based icing protection system that allows variation in operational voltage. The controllers are designed based on their respective derived plants for the main requirement of stable operation. The control scheme is tested in simulation to demonstrate the variable voltage concept along with the other operational capabilities.**

Keywords—more electric aircraft; variable dc bus voltage control; aircraft electrical power system

I. INTRODUCTION

The more electric aircraft (MEA) trend has been gaining traction through enabling technologies from power electronics and electrical machines. This type of aircraft aims to increase the reliance on electrical power on-board aircraft for load applications that have been traditionally been powered by pneumatic, hydraulic, or mechanical power. Such configuration may offer benefits in terms of design, prognostics, and efficiency [1, 2].

One of the aircraft loads is the icing protection systems, where various methods can be employed to prevent/remove ice on the flight surfaces. This can be done via mechanical boots, anti-freeze chemicals, bleed air from the aircraft engines, or heat from resistive elements (electro-thermal solution) [3, 4] where the latter would be in line with the MEA initiative. The use of resistive elements help save weight when compared to the current bleed air system as it reduces the need of heavy and inflexible pipes [3]. The reduced reliance on bleed air allows the engine to be more aerodynamically efficient [5]. Another advantage of using this method is that it does not pollute the environment or damage the wing structure.

The use of electro-thermal icing protection system (eIPS) requires large amounts of power in comparison to bleed air based systems. The B787 de-icing power consumption was reported to be between 45 to 75kW. If the system is set to anti-ice mode, the power demand increases drastically up to 200kW [4, 6]. This may limit the capability of the eIPS to be utilised on small surface areas of the aircraft depending on generator power availability. Dedicated electrical generators may be necessary to meet the eIPS power requirements [7].

As such, the electrical power generation system would have to undergo significant changes in the categories of power output density, power rating, and reliability to supply the increase in load demand [4]. The core modification is the exclusion of constant frequency gearbox commonly used in civil aircraft which thereby allows direct interface engine connection to the electrical generator. The variable frequency electrical power generated can then be regulated using power electronic converters.

One possible configuration between the generator system and the eIPS is interface connection via the main buses and have local converters/controllers to regulate the load power consumed. While this method is applicable, the amount of power may be limited by the constant bus voltage and current limit rating of the power converter. Another method is to establish a dedicated bus for the eIPS as seen in Fig. 1. This will ensure that other sensitive loads are not affected by the variable voltage levels. The bus voltage does not need to be fixed on the eIPS bus as the eIPS consists of mainly resistive loads. When the eIPS demands for very high power (i.e., anti-icing), then above rated voltage levels can be set and this is the variable voltage concept. An advantage of this topology is that it eliminates the need for local controllers which indirectly reduces the overall aircraft weight.

This paper introduces a control scheme that enables the variable voltage concept. The content is structured as follows; the power system is detailed in Section II and the proposed accompanying control scheme is described in Section III. Analysis and the design of the controllers are explained in Section IV, with the results and conclusions in Section V and VI respectively.

II. ELECTRICAL POWER SYSTEM

Fig. 1 shows the power system in study. A permanent magnet machine (PMM) is used as the main generator and is connected to a bi-directional AC-DC power converter. The

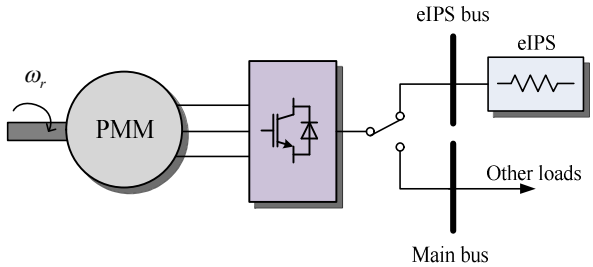

Fig. 1. Generator system with possible connection to eIPS bus or main bus.

converter can be connected to the main DC bus that feeds the various electrical loads or to a dedicated eIPS bus via a contactor. The eIPS can be represented as a purely resistive loads as its primary function is to generate heat for icing protection purposes. On the main bus are all other loads such as the environmental conditioning systems and cabin electrical equipment. While these loads are cut off when the eIPS is powered by the generator, it is assumed that the loads which are essential are powered by another source such as battery systems or auxiliary power unit. For this study, the power system is connected to the eIPS bus to enable the demonstration of the control scheme's full functionalities. The high level control that determines the bus connection is not considered in this paper.

The AC components of the power system are deduced in rotational reference *dq* frame [8]. Hence, the following are the main equation for the investigated power system:

$$v_d = R_s i_d + L_d \frac{di_d}{dt} - L_q \omega_e i_q \tag{1}$$

$$v_q = R_s i_q + L_q \frac{di_q}{dt} + \omega_e (L_d i_d + \psi_m) \tag{2}$$

$$E_{dc} i_{dc} = -\frac{3}{2}(v_d i_d + v_q i_q) \tag{3}$$

$$C \frac{dE_{dc}}{dt} = i_{dc} - \frac{E_{dc}}{R_w} \tag{4}$$

$v_{d,q}$ and $i_{d,q}$ are the PMM stator voltages and currents, $L_{d,q}$ are the PMM stator inductances, R_s is the stator resistance, ω_e is the electrical speed, and ψ_m is the machine flux. E_{dc} and i_{dc} are the bus voltages and currents, C is the bus capacitance, and R_w is the resistance of eIPS load.

III. Control Scheme

There are various functions that should be undertaken by the power system. The main tasks is bus voltage regulation (typically 270V for high voltage DC buses) to ensure that the electrical loads can operate nominally. The other task is to ensure that the current does not exceed the converter ratings limit. Flux weakening may be considered to maintain converter controllability when operating in high speed regions (up to 32,000rpm) [9]. Literature covering the controller design for the MEA generator systems has been covered in [9] and [10]. The control schemes in the literature were designed to accomplish the functionalities stated earlier, however another control scheme has to be considered for the variable voltage concept. In addition to the previous functionalities, the new control scheme has to regulate the power of the eWIPS load that will vary the bus voltage levels.

In principle, the variation of bus voltage levels changes the amount of power supplied to the eIPS via the equation:

$$P = \frac{V^2}{R} \tag{5}$$

where P is the power required by the eIPS, V is the bus voltage, and R is the eIPS total resistance. The concept is that if R is kept constant, then P can be increased if V increases.

Fig. 2 and Fig. 3 shows the proposed inner and outer control loops respectively. m_{abc} and m_{dq} are the modulation index in three phase and *dq* frame respectively. $m_{\lim}$ is the maximum modulation index and $m_{d\lim}$ is the limit imposed on m_d. i_{smax} and i_s are the stator current and its limit. P_{dc} is the DC power and k_s depends on the modulation scheme to be used for the power converter [11]. Variables with the superscript * denotes the reference values. The numbered i_q^* are corresponding to the outer loop controllers output.

The inner loops have two current controllers for the *dq* currents, W_{id} and W_{iq}. Feedforward compensation are also added to the outputs of the controllers and they are scaled to modulation indexes by $E_{dc}k_s$. A dynamic limit is used to employ flux weakening in this control scheme, whereby the modulation index should not exceed its limit following the equation:

$$m_{\lim} \geq \sqrt{m_d^{\,2} + m_q^{\,2}} \tag{6}$$

For this study, $m_{\lim}$ is set to 1 for full use of the available voltage [11]. When the limit is reached, i.e., within flux weakening region, the q-axis control loop shall determine the value for m_d which then introduces i_d as the reactive current to de-flux the PMM. Outside the flux weakening region, W_{id} is set to control i_d to 0. Another dynamic limit is used to ensure that v_q is within the limit when operating in flux weakening range:

$$v_{q\lim} = E_{dc} k_s \tag{7}$$

The outer control loop (Fig. 3) consists of three controllers to fulfil the functions of constant E_{dc}, P_{dc}, and i_{smax}. The E_{dc} controller, W_e, can be used to regulate the bus voltage to a constant value. It can also be used with the eIPS bus if only nominal power is required. The P_{dc} controller, W_p, is designed to control the power sent to the eIPS bus. This controller is setup for uni-directional power flow to only send power to the bus. The last controller, W_{is}, is for i_s limitation purpose as there is a lack of current restrictions present within the control scheme. When i_s exceeds its reference value, i_{q2}^* reduces in order to meet the following current limit:

$$i_{s\max} \geq \sqrt{i_d^{\,2} + i_q^{\,2}} \tag{8}$$

If i_s is less than i_{smax}, then W_{is} output is constrained to zero to prevent control conflicts. All the controllers are considered to be PI type with anti-windup scheme and more details of their design will be explained in the following Section. The output of these controllers can be used to determine i_q^*. The three signals are compared using a minimum function and the smallest value at a given time is selected as i_q^*. In general, the magnitude of error of the controllers determine the controller priority. The minimum function is used as it is assumed that the power flow from the PMM to the bus is negative, hence i_q is mainly negative. Back tracing is adapted in order to provide seamless transitions between the outer loop controllers [12]. This

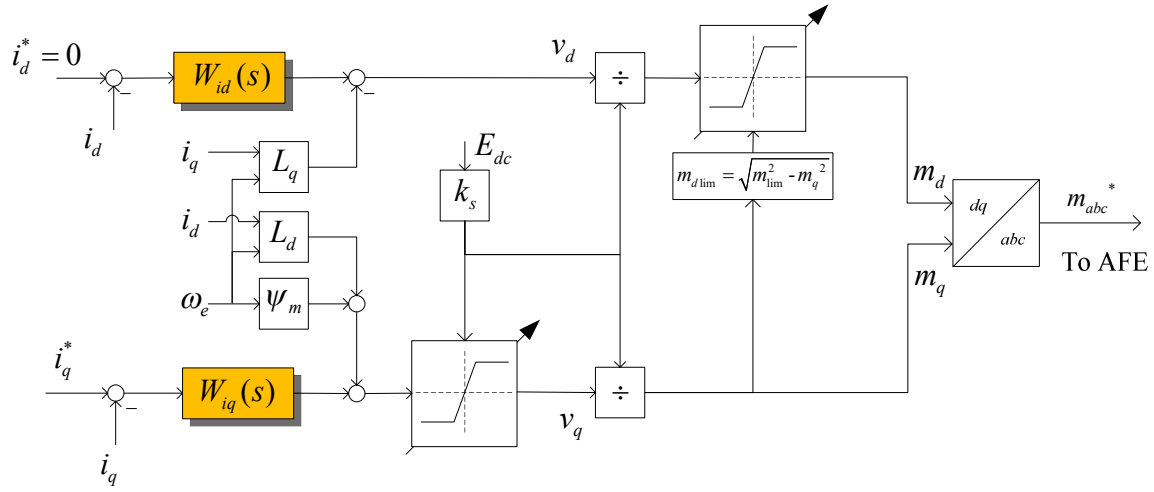

Fig. 2. Proposed inner control loop.

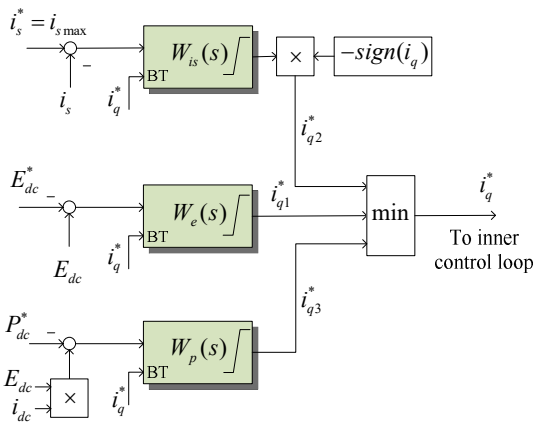

Fig. 3. Proposed outer control loop.

algorithm maintains all of the controllers' integrator states to be of similar value with respect to output i_q^*.

IV. Analysis

The control plants are derived in this Section to help with the controller design. The analysis is performed in small signal domain which only considers linear plants. Non-linear equations such as (6) and (8) are linearised using Taylor's approximation around a given operating point. The parameters used can be seen in TABLE I.

TABLE I. Power System Parameters

Parameter	Value
Stator resistance, R_s	$1.058m\Omega$
dq stator inductance, $L_d = L_q$	$99\mu H$
Pole pairs, p	3
Magnet flux-linkage, ψ_m	$0.03644Vs$
Rated power, P_{rated}	$40kW$
DC bus capacitance, C	$1.2mF$

It is assumed that ω_e is constant as the speed changes are much slower than the electrical components. The following are the small signal equations to be used to derive the outer control loop plants and their interactions can be shown in block diagram illustrated in Fig. 7.

$$\Delta v_d = R_s \Delta i_d + L_d s \Delta i_d - L_q \omega_{eo} \Delta i_q \tag{9}$$

$$\Delta v_q = R_s \Delta i_q + L_q s \Delta i_q + L_d \omega_{eo} \Delta i_d \tag{10}$$

$$m_{do} \Delta m_d = -m_{qo} \Delta m_q \tag{11}$$

$$\Delta i_s = \frac{i_{do}}{i_{so}} \Delta i_d + \frac{i_{qo}}{i_{so}} \Delta i_q \tag{12}$$

$$\Delta i_{dc} = \left[\begin{array}{l} -\frac{3}{2E_{dco}} (v_{do} \Delta i_d + i_{do} \Delta v_d + v_{qo} \Delta i_q + i_{qo} \Delta v_q) \\ +\frac{3}{2E_{dco}^2} (v_{do} i_{do} + v_{qo} i_{qo}) \Delta E_{dc} \end{array} \right] \tag{13}$$

$$\Delta E_{dc} = \frac{R_w}{CR_w s + 1} \Delta i_{dc} \tag{14}$$

$$\Delta P_{dc} = i_{dco} \Delta E_{dc} + E_{dco} \Delta i_{dc} \tag{15}$$

$$\Delta v_d = k_s m_{do} \Delta E_{dc} + k_s E_{dco} \Delta m_d \tag{16}$$

$$\Delta v_q = k_s m_{qo} \Delta E_{dc} + k_s E_{dco} \Delta m_q \tag{17}$$

Any variable with the o subscript denotes its initial operating point value. The inner current loop design has been discussed in details in [8] and the controller has been designed to achieve 500Hz bandwidth and 0.7 damping factor. The closed loop transfer function for i_q is:

$$\frac{\Delta i_q}{\Delta i_q^*} = \frac{k_{pq} s + k_{iq}}{L_q s^2 + (R_s + k_{pq}) s + k_{iq}} \tag{18}$$

where k_{pq} and k_{iq} are the proportional and integral terms of W_{iq}.

A. E_{dc} control loop

The plant for this control loop should relate input Δi_q^* to ΔE_{dc}. Using equation (13), each small signal term can be replaced with the other linear equations so that the plant can be found as:

$$\frac{\Delta E_{dc}}{\Delta i_q^*} = \frac{-3E_{dco} R_w (a_{1e} s^2 + a_{2e} s + a_{3e})}{(b_{1e} s^2 + b_{2e} s + b_{3e})} \frac{\Delta i_q}{\Delta i_q^*} \tag{19}$$

The coefficients for a_{1e}, a_{2e}, a_{3e}, b_{1e}, b_{2e}, and b_{3e} are located in the Appendix section. This linear plant is verified with an equivalent non-linear model built in Simulink via step response comparison. Hence, the derived transfer function can be used to represent the plant for E_{dc}.

The bode plot at different loads were also plotted as depicted in Fig. 4. As the load power increases more than 10kW, there is a tendency for the phase angle to exceed -180º which may cause instability when the closed loop gain is within that region. At higher frequencies the plant stabilises back again. Therefore, the plant at full load should be considered for the control design of W_e to take into account the unstable region. The gain margin at each load variation was found to be similar at about 21.8dB at the -180º crossover point. As long as the controller gain is selected to be within the gain margin, stability is ensured. This gain margin (up to k =12.3) is verified via a non-linear model built in Simulink and the instability is recorded when the controller gain is changed in Fig. 5.

B. P_{dc} control loop

From (15), it can be seen that the P_{dc} plant will relate closely to the newly derived E_{dc} plant. Combining (14), (15), and (19) yields:

$$\frac{\Delta P_{dc}}{\Delta i_q^*} = (E_{dco} C R_w s + i_{dco} R_w + E_{dco}) \frac{\Delta E_{dc}}{\Delta i_q^*} \frac{\Delta i_q}{\Delta i_q^*} \quad (20)$$

The derived transfer function was also verified with an equivalent non-linear model. Fig. 6 shows the closed loop bode plots at different loads with a pure integral controller. The phase margin for 40kW was observed to be more than 180º, which indicates non-minimum phased characteristics. This would mean that the controller will have a limited gain range that allows stable operation. The gain margin at the 180º crossover was found to be 29.5 dB, which can be used as a reference during the controller design for this power system. If a proportional term is added to W_p, the gain has to be very small due to the resolution of the control variable (power in the order of 10^4) to the output i_q (within 10^2). Hence, the proportional term can be omitted in order to simplify the control design process for W_p.

C. i_s control loop

Since the stator current is the control variable for this loop, hence the plant can be derived from the linearised current limit equation (12). Using the equations (9) to (18), the i_s plant can be derived to be:

$$\frac{\Delta i_s}{\Delta i_q^*} = \frac{a_{1i} s^2 + a_{2i} s + a_{3i}}{i_{so}(b_{1i} s^2 + b_{2i} s + b_{3i})} \frac{\Delta i_q}{\Delta i_q^*} \quad (21)$$

Similar to the previous analysis, the bode plot for this plant has been illustrated in Fig. 8 at operating loads up to 40kW. The phase does exceed 180º which indicates non-minimum phase as well. The gain margin was found to be 19.5dB at the highest load point and W_{is} is selected such that its gains are within the margin.

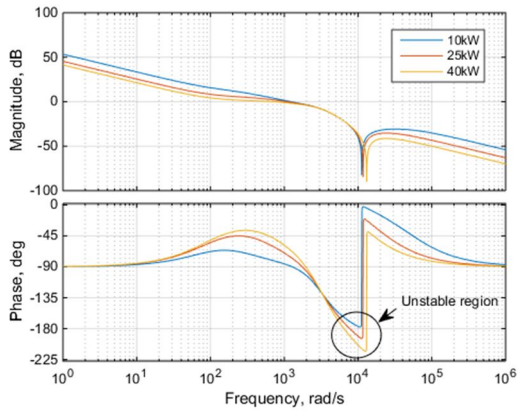

Fig. 4. E_{dc} plant with PI controller bode plot at different load levels.

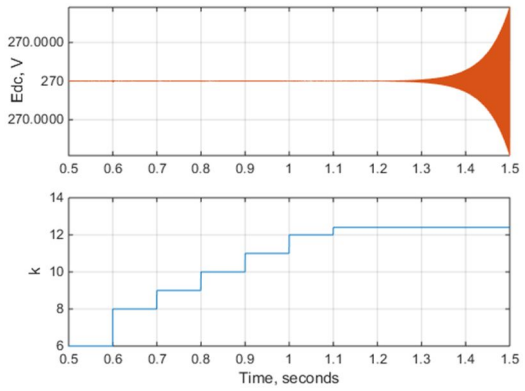

Fig. 5. E_{dc} response to changes of W_e gain up to k = 12.5.

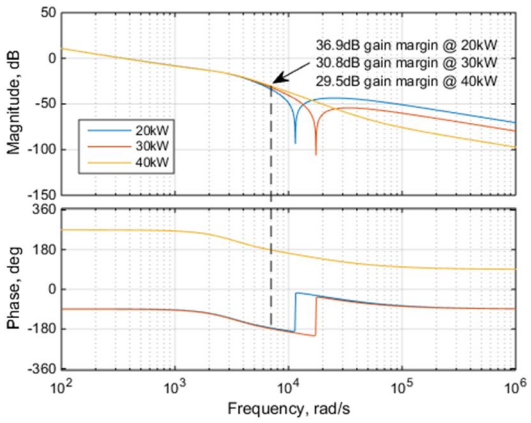

Fig. 6. P_{dc} plant with I controller bode plot at different load levels.

Based on the analysis in this Section, both P_{dc} and i_s plants have clear indication of non-minimum phase characteristics and their controllers should be designed carefully for stable operation. The selection of full load operating point for small signal analysis along with the linearised plants can help with the control design process. The following gains have been selected for the outer loop controllers to achieve reasonable bandwidth response within the stable margins and they are shown in TABLE II. The back-tracing gains for the outer loop control have been selected as 150 to realise fast tracking during changes of controller output.

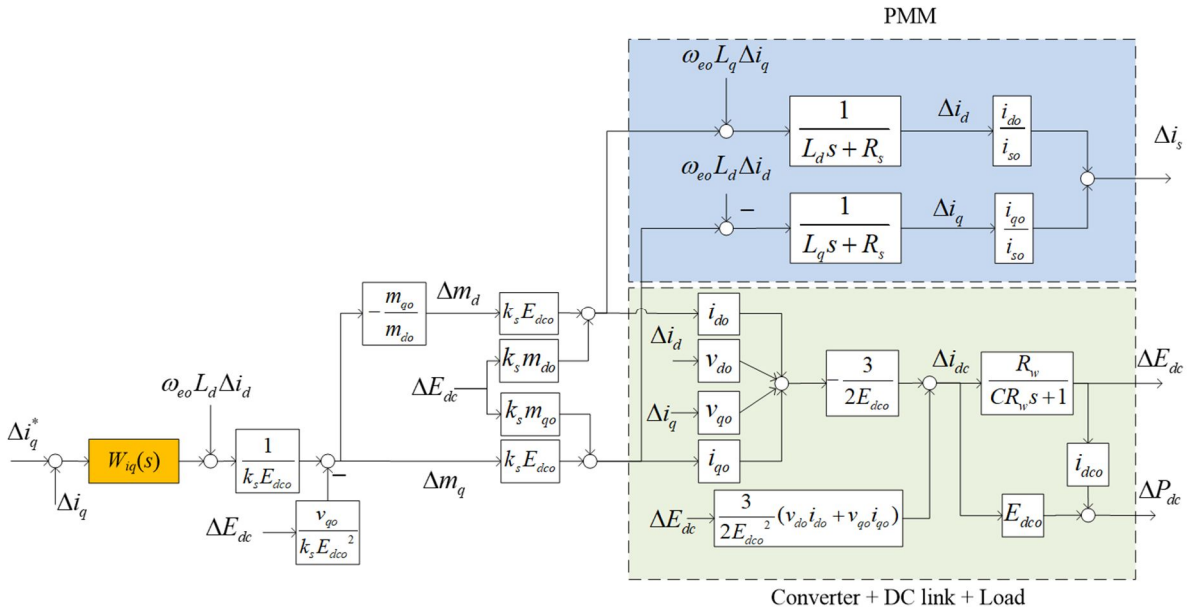

Fig. 7. Linearised equations forming the plants for E_{dc}, P_{dc}, and i_s.

V. Simulation Results

The time domain simulation results showing function of the proposed control scheme can be seen in Fig. 9 and Fig. 10. The operating points were selected such that the operation of each outer loop controllers are distinct. The simulation started with ω_r = 20krpm, m_{lim} = 1, P_{dc}^* = 20kW, R_w = 25kW at 270V, and the i_{smax} = 150A.

At t = 0.1s and 0.2s, there is incremental step increase of P_{dc}^* = 3kW applied to demonstrate the function of W_p. During this period, it can be observed in the figures that W_p is online as its output, i_{q3}^*, fulfils the minimum function and P_{dc} is controlled to the respective demand. As a result, E_{dc} increases in order to satisfy the power demand, obeying equation (5). The power reduction can be observed at t = 0.7s and 0.8s respectively until P_{dc}^* is lower than the nominal power consumed by R_w and W_e resumes control of E_{dc} = 270V (t > 0.8s). The role of W_e is to maintain constant E_{dc} if the other two controllers are not given priority.

At t = 0.3s, the speed was increased by 2krpm in order to increase i_s demand and to test the operation of W_{is}. This mainly increases the demand of i_d for flux weakening to maintain m = 1 as the speed goes higher. Eventually, i_s is limited to be within 150A and with an initial overshoot. The overshoot can be contained but can be difficult to be eliminated. Fortunately, this control scheme allows some level of current overshoot and throughout the operation, m has been kept at 1 using the modulation index limit.

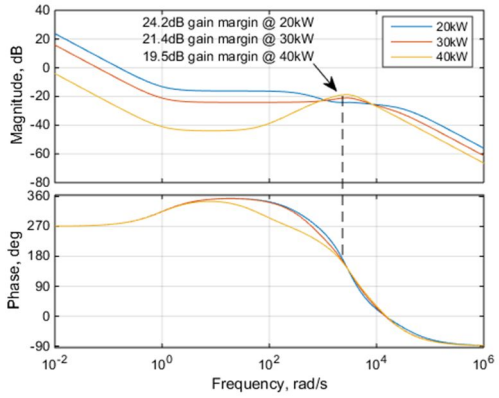

Fig. 8. i_s plant with PI controller bode plot at different load levels.

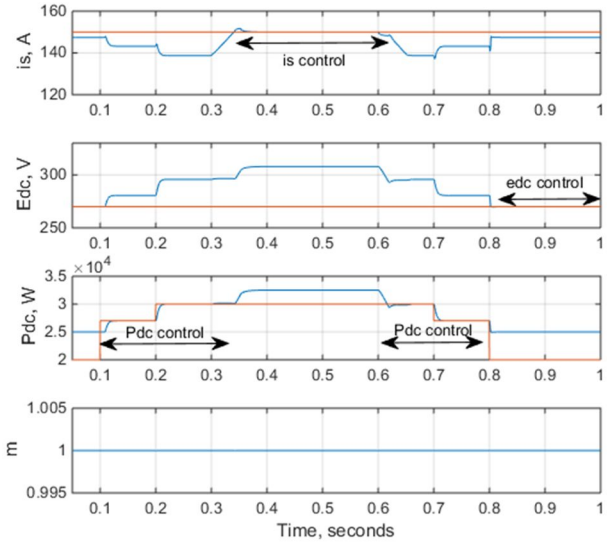

Fig. 9. Time domain simulation demonstrating the variable voltage control concept.

The changes between the outer loop controllers can be observed through i_q^*. In Fig. 10, it can be seen that the controller output that demands the largest i_q (in the negative direction) is selected for i_q^*. Moreover, slightly different transient dynamics can be seen in E_{dc}, P_{dc}, and i_s between the changed and reverted operating points. This is due to the differences in their controller bandwidth response.

VI. Conclusion

The variable voltage concept has been studied for the MEA electrical power system with eIPS as its load. The control scheme can perform constant E_{dc} control if connected to a main bus, P_{dc} control for power variation in the eIPS, i_s control for overall current limit, and flux weakening by restricting the

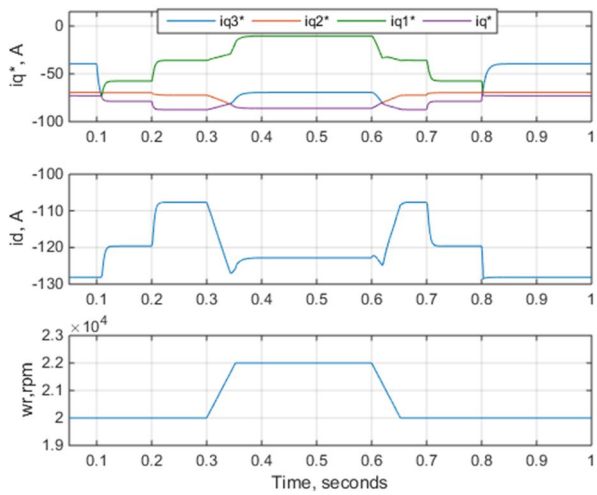

Fig. 10. i_q^*, i_d, and ω_r with respect to Fig. 9.

modulation index. Small signal transfer functions have been derived to aid with the controller design process. Non-minimum phase was detected within the P_{dc} and i_s plants as indicated by their phase exceeded 180º. This meant that the controllers would have to be designed carefully for stable operation. Simulations have been performed to demonstrate the functionalities of the control scheme. Future studies would include experimental validation with a prototype MEA generator system and extensive investigation of its stability.

TABLE II. OUTER LOOP CONTROLLER GAINS

Control loop	Controller gains
E_{dc}	$k_p = 1.5$
	$k_i = 300$
P_{dc}	$k_p = 0$
	$k_i = 1$
i_s	$k_p = 0.5$
	$k_i = 200$

ACKNOWLEDGEMENT

This project has received funding from the Clean Sky 2 Joint Undertaking under the European Union's Horizon 2020 research and innovation programme under grant agreement No CS2-AIR-GAM-2014-2015-01. Cf. Art.29.4 of [A2].

REFERENCES

[1] B. Sarlioglu and C. T. Morris, "More Electric Aircraft: Review, Challenges, and Opportunities for Commercial Transport Aircraft," *IEEE Trans. Transport. Elec.,* vol. 1, pp. 54-64, 2015.

[2] P. Wheeler and S. Bozhko, "The More Electric Aircraft: Technology and challenges," *Electrification Magazine, IEEE,* vol. 2, pp. 6-12, 2014.

[3] Z. Goraj, "An Overview of the De-Icing and Anti-Icing Technologies with Prospects for the Future," presented at the 24th Congress of International Council of the Aeronautical Sciences ICAS, Yokohama, Japan, 2004.

[4] I. Moir and A. Seabridge, *Aircraft Systems: Mechanical, Electrical and Avionics Subsystems Integration*: Wiley, 2008.

[5] A. Abdel-Hafez, *Power Generation and Distribution System for a More Electric Aircraft - A Review, Recent Advances in Aircraft Technology*, 2012.

[6] J. Sloan. (2008). *787 integrates new composite wing deicing system*. Available: https://www.compositesworld.com/articles/787-integrates-new-composite-wing-deicing-system. Accessed: 7/3/2018

[7] A. C. Kodet, "Electro-impulse deicing," in *Proceedings of the IEEE Southern Tier Technical Conference*, 1988, pp. 193-200.

[8] P. C. Krause, O. Wasynczuk, S. D. Sudhoff, and I. P. E. Society, *Analysis of electric machinery and drive systems*: IEEE Press, 2002.

[9] S. S. Yeoh, F. Gao, S. Bozhko, and G. Asher, "Control design for PMM-based starter generator system for More Electric Aircraft," in *Power Electronics and Applications (EPE'14-ECCE Europe)*, 2014, pp. 1-10.

[10] F. Gao, S. Bozhko, A. Costabeber, G. Asher, and P. Wheeler, "Control Design and Voltage Stability Analysis of a Droop-Controlled Electrical Power System for More Electric Aircraft," *IEEE Transactions on Industrial Electronics,* vol. 64, pp. 9271-9281, 2017.

[11] A. Yazdani and R. Iravani, *Voltage-Sourced Converters in Power Systems*: John Wiley & Sons, Inc., 2010.

[12] H. B. Enalou and E. A. Soreshjani, "A Detailed Governor-Turbine Model for Heavy-Duty Gas Turbines With a Careful Scrutiny of Governor Features," *IEEE Transactions on Power Systems,* vol. 30, pp. 1435-1441, 2015.

APPENDIX

$$a_{1e} = L_d L_q \left(i_{qo} m_{do} - i_{do} m_{qo} \right)$$

$$a_{2e} = R_s i_{qo} m_{do} \left(L_d + L_q \right) - R_s i_{do} m_{qo} \left(L_d + L_q \right) - L_q m_{qo} v_{do} + L_d m_{do} v_{qo}$$

$$a_{3e} = -R_s m_{qo} v_{do} + R_s m_{do} v_{qo} + L_q m_{do} v_{do} \omega_{eo} + L_d m_{qo} v_{qo} \omega_{eo}$$
$$+ i_{qo} m_{do} \left(R_s^2 + L_d L_q \omega_{eo}^2 \right) - i_{do} m_{qo} \left(R_s^2 + L_d L_q \omega_{eo}^2 \right)$$

$$b_{1e} = 2CE_{dco}^2 L_d R_w m_{do}$$

$$b_{2e} = 3E_{dco} i_{do} k_s L_d R_w \left(m_{do}^2 + m_{qo}^2 \right) - 3L_d m_{do} R_w \left(i_{do} v_{do} + i_{qo} v_{qo} \right)$$
$$+ 2E_{dco}^2 \left(R_s C m_{do} R_w + L_d \left(m_{do} + C m_{qo} R_w \omega_{eo} \right) \right)$$

$$b_{3e} = 3E_{dco} k_s R_w \left(m_{do}^2 + m_{qo}^2 \right) \left(R_s i_{do} + v_{do} + i_{qo} L_d \omega_{eo} \right)$$
$$+ 2E_{dco}^2 \left(R_s m_{do} + L_d m_{qo} \omega_{eo} \right) - 3R_w \left(i_{do} v_{do} + i_{qo} v_{qo} \right) \left(R_s m_{do} + L_d m_{qo} \omega_{eo} \right)$$

$$a_{1i} = 2CE_{dco}^2 R_w \left(i_{qo} L_d m_{do} - i_{do} L_q m_{qo} \right)$$

$$a_{2i} = 3E_{dco} i_{do} i_{qo} k_s R_w \left(L_d - L_q \right) \left(m_{do}^2 + m_{qo}^2 \right)$$
$$+ 3R_w \left(-i_{qo} L_d m_{do} + i_{do} L_q m_{qo} \right) \left(i_{do} v_{do} + i_{qo} v_{qo} \right)$$
$$+ 2E_{dco}^2 \begin{pmatrix} -i_{do} \left(R_s C m_{qo} R_w + L_q \left(m_{qo} - C m_{do} R_w \omega_{eo} \right) \right) \\ + i_{qo} \left(R_s C m_{do} R_w + L_d \left(m_{do} + C m_{qo} R_w \omega_{eo} \right) \right) \end{pmatrix}$$

$$a_{3i} = 2E_{dco}^2 \left(i_{do} \left(-R_s m_{qo} + L_q m_{do} \omega_{eo} \right) + i_{qo} \left(R_s m_{do} + L_d m_{qo} \omega_{eo} \right) \right)$$
$$+ 3E_{dco} k_s R_w \left(m_{do}^2 + m_{qo}^2 \right) \left(i_{qo} v_{do} + i_{qo}^2 L_d \omega_{eo} + i_{do} \left(-v_{qo} + i_{do} L_q \omega_{eo} \right) \right)$$
$$+ 3R_w \left(i_{do} v_{do} + i_{qo} v_{qo} \right) \begin{pmatrix} i_{do} \left(R_s m_{qo} - L_q m_{do} \omega_{eo} \right) \\ - i_{qo} \left(R_s m_{do} + L_d m_{qo} \omega_{eo} \right) \end{pmatrix}$$

$$b_{1i} = 2CE_{dco}^2 L_d R_w m_{do}$$

$$b_{2i} = 3E_{dco} i_{do} k_s L_d R_w \left(m_{do}^2 + m_{qo}^2 \right) - 3L_d m_{do} R_w \left(i_{do} v_{do} + i_{qo} v_{qo} \right)$$
$$+ 2E_{dco}^2 \left(R_s C m_{do} R_w + L_d \left(m_{do} + C m_{qo} R_w \omega_{eo} \right) \right)$$

$$b_{3i} = 3E_{dco} k_s R_w \left(m_{do}^2 + m_{qo}^2 \right) \left(R_s i_{do} + v_{do} + i_{qo} L_d \omega_{eo} \right)$$
$$+ 2E_{dco}^2 \left(R_s m_{do} + L_d m_{qo} \omega_{eo} \right) - 3R_w \left(i_{do} v_{do} + i_{qo} v_{qo} \right) \left(R_s m_{do} + L_d m_{qo} \omega_{eo} \right)$$